Chapter 2

Methods for Improving the Performance of an SAR Recognition System

Bir Bhanu[1] and Grinnell Jones III[2]

[1] Center for Research in Intelligent Systems, University of California, Riverside, California 92521, bhanu@cris.ucr.edu
[2] Center for Research in Intelligent Systems, University of California, Riverside, California 92521, grinnell@cris.ucr.edu

Summary. The focus of this chapter is on methods for improving the performance of a model-based system for recognizing vehicles in synthetic aperture radar (SAR) imagery under the extended operating conditions of object articulation, occlusion, and configuration variants. The fundamental approach uses recognition models based on quasi-invariant local features, radar scattering center locations, and magnitudes. Three basic extensions to this approach are discussed: (1) incorporation of additional features; (2) exploitation of a priori knowledge of object similarity represented and stored in the model-base; and (3) integration of multiple recognizers at different look angles. Extensive experimental recognition results are presented in terms of receiver operating characteristic (ROC) curves to show the effects of these extensions on SAR recognition performance for real vehicle targets with articulation, configuration variants, and occlusion.

2.1 Introduction

In this chapter we are concerned with methods for improving the recognition of vehicles in Synthetic Aperture Radar (SAR) imagery. The recognition systems start with real SAR chips (at one foot resolution) of actual military vehicles from the MSTAR public data [1] and end with the identification of a specific vehicle type (e.g., a T72 tank). Several major challenges for identifying the vehicles are the presence of significant external configuration variants (fuel barrels, searchlights, etc.), articulated configurations (such as a tank with its turret rotated), and partial occlusion. The detection theory [2, 3], pattern recognition [4, 5, 6], and neural network [7] approaches to SAR recognition all tend to use global features that are optimized for standard, non-articulated, non-occluded configurations. Approaches that rely on global features are not appropriate for recognizing occluded or articulated objects because occlusion and articulation change global features like the object outline and major axis [8]. Our previous work [9, 10, 11, 12], relied on local features to successfully recognize articulated and highly occluded objects. SAR recognition results for

our basic approach are compared (in [9]) to other different approaches using real SAR images from the MSTAR public data.

In our research on SAR automatic target recognition (ATR), we initially started using invariant locations of SAR scattering centers as features [12] and later developed our basic recognition approach based on using quasi-invariant locations and magnitudes of the scattering centers [9, 10, 11]. This followed the traditional approach to improving recognition performance by finding additional features that can help to distinguish between the objects. This is the first method of improvement discussed in this chapter. The second method of exploiting model similarity was inspired by the research on predicting the performance of recognition systems by Boshra and Bhanu [13] that introduced the idea that recognition performance depends on the distortion in the test data and the inherent similarity of the object models. Related to the third method for improving recognition performance, we had previously shown that a significant number of SAR scattering center locations do not typically persist over a few degrees of rotation [10]. However, this had been viewed as a problem for modeling, rather than a potential opportunity for independent observations at different look angles. In this chapter, we integrate results from multiple look angles to improve recognition performance.

This chapter discusses three basic approaches to improve the performance of an SAR recognition system:

1. Incorporation of additional features.
2. Exploitation of a priori knowledge of object similarity.
3. Integration of multiple recognizers at different look angles.

The next section discusses SAR target characteristics; Section 2.3 gives a description of the basic SAR recognition system; Section 2.4 introduces the additional feature of peak shape factor and shows performance improvements for additional features; Section 2.5 describes techniques to measure and utilize model similarity to improve recognition performance; Section 2.6 demonstrates the independence of multiple look angle SAR recognition and the results for performance improvements; and the final Section 2.7 provides the conclusions of the chapter.

2.2 SAR Target Characteristics

The typical detailed edge and straight line features of man-made objects in the visual world do not have good counterparts in SAR images for subcomponents of vehicle-sized objects at one-foot resolution. However, there is a wealth of peaks corresponding to scattering centers. The relative locations of SAR scattering centers, determined from local peaks in the radar return, are related to the aspect and physical geometry of the object, independent of translation and serve as distinguishing features. Target regions-of-interest (ROI) are found in the MSTAR SAR chips by reducing speckle noise using

the Crimmins algorithm (see [14]), thresholding at the mean plus two standard deviations, dilating to fill small gaps among regions, eroding to have one large ROI and little regions, discarding the small regions with a size filter and dilating to expand the extracted ROI. The scattering centers are extracted from the SAR magnitude data (within the boundary contour of the ROI) by finding local eight-neighbor maxima. The parameters used in extracting ROIs are held constant for all the results reported.

Objects from the MSTAR public data used in this research include: BMP2 armored personnel carriers (APCs), a BTR70 APC, T72 tanks, a ZSU23/4 anti-aircraft gun, and a BRDM2 APC. Photo images of the MSTAR articulated objects used in this paper, T72 tank serial number (#) a64 and ZSU 23/4 anti-aircraft gun #d08, are shown in Figures 2.1 and 2.2. Example SAR images and the ROI, with the locations of the scattering centers superimposed are shown in Figure 2.3 for baseline and articulated versions of the T72 and ZSU (at 30° radar depression angle, 66° target azimuth).

(a) turret straight. (b) turret articulated.

Figure 2.1. T72 tank #a64.

(a) turret straight. (b) turret articulated.

Figure 2.2. ZSU 23/4 anti-aircraft gun #d08.

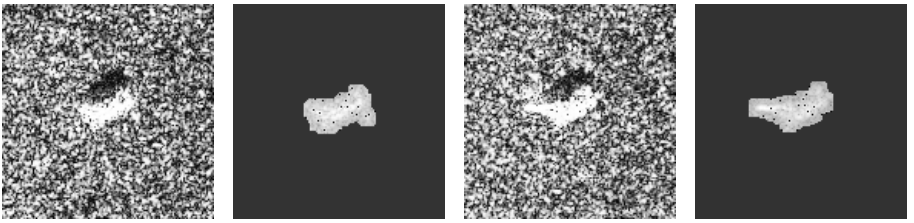

(a) T72: image. (b) ROI. (c) articulated image. (d) articulated ROI.

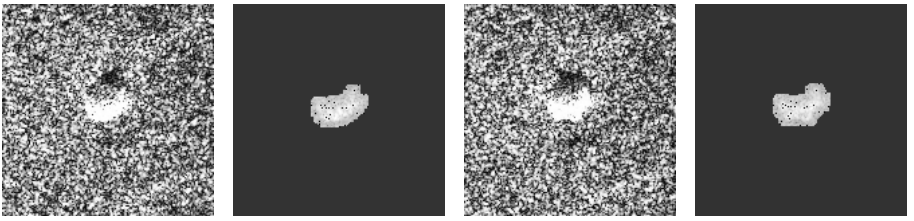

(a) ZSU: image. (b) ROI. (c) articulated image. (d) articulated ROI.

Figure 2.3. MSTAR SAR images and ROIs (with peaks) for T72 tank #a64 and ZSU 23/4 #d08 at 66° azimuth.

2.2.1 Azimuthal Variance of Scatterer Locations

The typical rigid body rotational transformations for viewing objects in the visual world do not apply much for the specular radar reflections of SAR images. This is because a *significant* number of features *do not* typically persist over a few degrees of rotation. Since the radar depression angle is generally known, the significant unknown target rotation is (360°) in azimuth. Azimuth persistence or invariance can be expressed in terms of the percentage of scattering center locations that are unchanged over a certain span of azimuth angles. It can be measured (for some base azimuth θ_o) by rotating the pixel locations of the scattering centers from an image at azimuth θ_o by an angle $\Delta\theta$ and comparing the resulting range and cross-range locations with the scatterer locations from an image of the same object at azimuth $\theta_0 + \Delta\theta$. More precisely, because the images are in the radar slant plane, we actually project from the slant plane to the ground plane, rotate in the ground plane, and project back to the slant plane. Since the objects in the chips are not registered, we calculate the azimuth invariance as the maximum number of corresponding scattering centers (whose locations match within a given tolerance) for the optimum integer pixel translation. This method of registration by finding the translation that yields the maximum number of correspondences has the limitation that for very small or no actual invariance it may find some false correspondences and report a slightly higher invariance than in fact exists. To determine scattering center locations that persist over a span of angles, there is an additional constraint that for a matching scattering center

to "persist" at the kth span $\Delta\theta_k$, it must have been a persistent scattering center at all smaller spans $\Delta\theta_j$, where $0 \leq j < k$. Averaging the results of these persistent scattering center locations over 360 base azimuths gives the mean azimuth invariance of the object.

Figure 2.4 shows an example of the mean azimuth invariance (for the 40 strongest scatterers) as a function of azimuth angle span using T72 tank #132, with various definitions of persistence. In the "exact match" cases the center of the rotated scatterer pixel from the image at θ_o azimuth is within the pixel boundaries of a corresponding scatterer in the image at $\theta_0 + \Delta\theta$. In the "within 1 pixel" cases, the scatterer location is allowed to move into one of the 8 adjacent pixel locations. Note that for a 1° azimuth span, while only 20% of the scatterer locations are invariant for an "exact match," 65% of the scatterer locations are invariant "within 1 pixel." The cases labeled "persists" in Figure 2.4 enforce the constraint that the scatterer exist for the entire span of angles and very few scatterers continuously persist for even 5°. In the upper two cases (not labeled "persists") scintillation is allowed and the location invariance declines slowly with azimuth span. The "within 1 pixel" results (that allow scintillation) are consistent with the one-foot ISAR results of Dudgeon *et al.* [15], whose definition of persistence allowed scintillation. Because of the higher scatterer location invariance with 1° azimuth span, in our research we use azimuth models at 1° increments for each target, in contrast to others who have used 5° [16], 10° [17], and 12 models covering specific azimuth ranges [6].

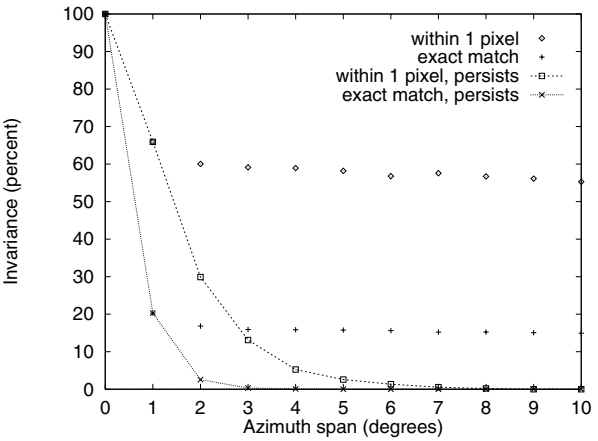

Figure 2.4. Scatterer location persistence, T72 #132.

The fact that the SAR scatterer locations *do not* persist over a span of even a few degrees, demonstrated in Figure 2.4, strongly indicates that observations at different azimuth angles are independent. Thus, what had previously been viewed as a "problem" for modeling, now presents a significant opportunity

to improve recognition performance by integrating the results of SAR observations at multiple look angles. This is the basis for the approach which will be discussed later in Section 2.6.

2.2.2 Scatterer Location and Magnitude Invariance

Many of the scatterer locations and magnitudes are invariant to target conditions such as articulation or configuration variants. Because the object and ROI are not registered, we express the scattering center location invariance with respect to articulation or configuration differences as the maximum number of corresponding scattering centers (whose locations match within a stated tolerance) for the optimum integer pixel translation.

Figure 2.5 shows the location invariance of the strongest 40 scattering centers with articulation for T72 tank #a64 and also for ZSU 23/4 anti-aircraft gun #d08 (at a 30° depression angle) as a function of the hull azimuth. The combined average invariance for both articulated vehicles is 16.5% for an exact match of scattering centers and 56.5% for a location match within one pixel (3x3 neighborhood) tolerance. (Note that not all 360 degrees are present in the MSTAR data, so the missing azimuth angles are ignored in this research.) Similarly, Figure 2.6 shows the percent of the strongest 40 scattering center locations that are invariant for two example configuration variants, T72 #812 vs. #132 and BMP2 vehicle #9563 vs. #C21, at a 15° depression angle. (While the MSTAR data has 11 configurations of the T72, it only has three configurations of the BMP2, so to avoid biasing the experiments toward the T72, we use only three of the T72 configurations.) The combined average invariance for configuration variants of the T72 (#812 and #s7 vs. #132) and BMP2 (#9563 and #9566 vs. #c21) is 15.3% for an exact match of scatterer locations and 57.15% for a location match within one pixel. Since less than 20% of the SAR scattering center locations exactly match for object articulation and configuration variants, while over 50% of these locations are quasi-invariant within a 3∗3 pixel tolerance, in our research we accommodate this 3∗3 tolerance for scattering center locations in the recognition system.

Because of the very large dynamic range for scatterer magnitudes we use a scaled scatterer amplitude (S), expressed as a radar cross-section in square meters, given by $S = 100 + 10\log_{10}(i^2 + q^2)$, where i and q are the components of the complex radar return, and we define a percent amplitude change (A_{jk}) as: $A_{jk} = 100(S_j - S_k)/S_j$. Note that this form allows a larger variation for the stronger signal returns. Figure 2.7 shows the probability mass functions (PMFs) for percent amplitude change for the strongest 40 articulated vs. nonarticulated scattering centers of T72 tank #a64 and ZSU 23/4 gun #d08. Curves are shown both for the cases where the scattering center locations correspond within one pixel tolerance and for all the combinations of scatterers whose locations do not match. Similarly, Figure 2.8 shows the PMFs for percent amplitude change for the strongest 40 scattering centers with configuration variants, T72 #812 vs. #132 and BMP2 #9563 vs. #C21,

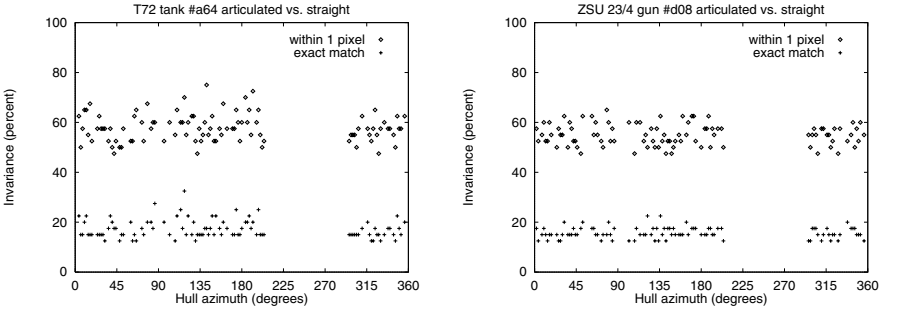

(a)T72 tank. (b)ZSU 23/4.

Figure 2.5. Scatterer location invariance with articulation.

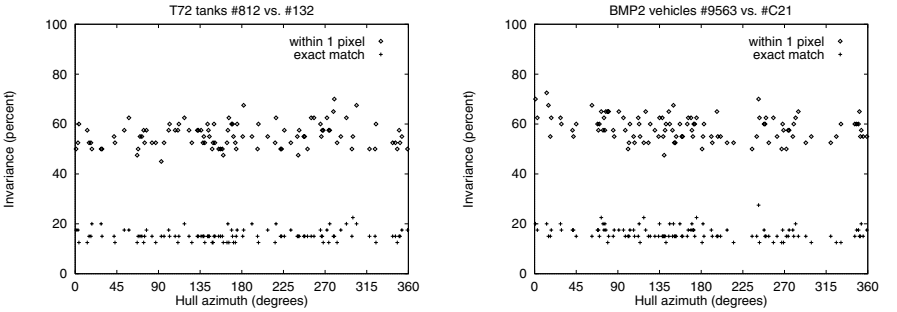

(a)T72 tank. (b)BMP2.

Figure 2.6. Scatterer location invariance with configuration.

at a 15° depression angle. If we define scatterer *magnitude invariance* as the number of scatterers with corresponding locations whose magnitudes match (within a stated percent amplitude change tolerance), then the overall average scatterer magnitude invariance (within ± one pixel location and ± nine percent amplitude change) is 50.8 percent for the articulation cases and 51.7 percent for the configuration variant cases.

2.2.3 Target Occlusion

There is no real SAR data with occluded objects available to the general public (limited data on vehicles in revetments [18] and partially hidden behind walls [19] has been reported to exist, but it has not yet been released for unrestricted use). In addition, there is no standard, accepted method for characterizing or simulating occluded targets. Typically occlusion occurs when a tank backs up into a tree line, for example, so that the back end is covered by trees and only the front portion of the tank is visible to the radar. Thus, the "bright target" becomes a much smaller sized object to the recognition

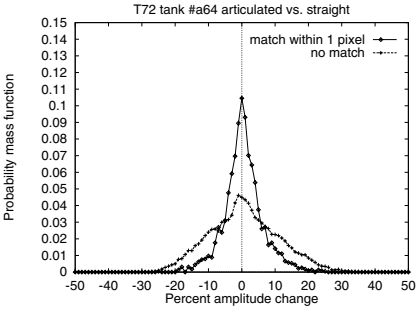

(a)T72 tank.

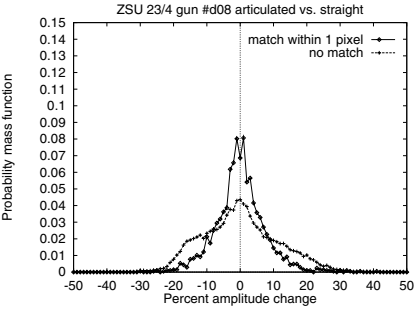

(b)ZSU 23/4.

Figure 2.7. Scatterer magnitude invariance with articulation.

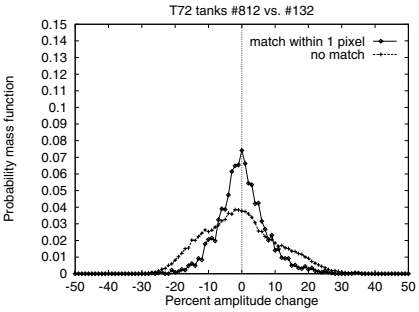

(a)T72 tank.

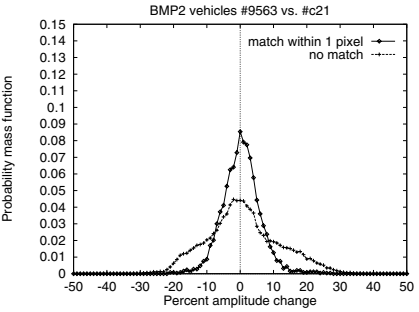

(b)BMP2.

Figure 2.8. Scatterer magnitude invariance with configuration.

system. In addition, the tree tops can produce "bright" peaks that are similar to the strength of target peaks at many azimuths.

The occluded test data in our research is simulated by starting with a given number of the strongest scattering centers and then removing the appropriate number of scattering centers encountered in order, starting in one of four perpendicular directions d_i (where d_1 and d_3 are the cross-range directions, along and opposite the flight path, respectively, and d_2 and d_4 are the up range and down range directions). Then the same number of scattering centers (with random magnitudes) are added back at *random locations* within the original bounding box of the chip. This keeps the number of scatterers constant and acts as a surrogate for some potential occluding object. Our approach, using simulated occlusion provides an enormous amount of data with varying known amounts of occlusion for carefully controlled experiments.

2.3 Basic SAR Recognition System

The basic SAR recognition algorithm is an off-line model construction process and a similar on-line recognition process. The approach is designed for SAR and is specifically intended to accommodate recognition of occluded and articulated objects. Standard nonarticulated models of the objects are used to recognize these same objects in nonstandard, articulated, and occluded configurations. The models are a look-up table and the recognition process is an efficient search for positive evidence, using relative locations of the scattering centers in the test image to access the look-up table and generate votes for the appropriate object (and azimuth pose).

Establishing an appropriate local coordinate reference frame is critical to reliably identifying objects (based on locations of features) in SAR images of articulated and occluded objects. These problems require the use of a local coordinate system; global coordinates and global constraints do not work, as illustrated in Figure 2.3, where the center of mass and the principal axes change with articulation. In an SAR image the radar range and cross-range directions are known and choosing any local reference point, such as a scattering center location, establishes a reference coordinate system. The relative distance and direction of the other scattering centers can be expressed in radar range and cross-range coordinates, and naturally tessellated into integer buckets that correspond to the radar range/cross-range bins. The scale is determined by the bin size, which is a function of the frequency of the radar (e.g., X-band for the one foot resolution used in this research). The recognition system takes advantage of this natural system for SAR, where a single basis point performs the translational transformation and fixes the coordinate system to a "local" origin.

The model construction algorithm for the recognition system is outlined in Figure 2.9 (where the "origin" is the stronger of a pair of scatterers and a "point" is another weaker scatterer). Because of the specular radar reflections in SAR images, a significant number of features do not typically persist over a few degrees of rotation (as shown in Figure 2.4). Consequently, we model each object at 1° azimuth increments. The relative locations and magnitudes of the N strongest SAR scattering centers are used as characteristic features (where N, the number of scattering centers used, is a design parameter). Any local reference point, such as a scattering center location, could be chosen as a basis point ("origin") to establish a reference coordinate system for building a model of an object at a specific azimuth angle pose. For ideal data, picking the location of the strongest scattering center as the origin is sufficient. However, for potentially corrupted data where any scattering center could be spurious or missing (due to the effects of noise, target articulation, occlusion, nonstandard target configurations, etc.), we use all N strongest scattering centers in turn as origins to ensure that a valid origin is obtained. Thus, to handle occlusion and articulation, the size of the look-up table models (and also the number of relative distances that are considered in the test image during

recognition) are increased from N to $N(N-1)/2$. Using a technique like geometric hashing [20], the models are constructed using the relative positions of the scattering centers in the range (R) and cross-range (C) directions as the initial indices to a look-up table of labels that give the associated target type, target pose, "origin" range and cross-range positions, and the magnitudes (S) of the two scatterers. Since the relative distances are not unique, there can be several of these labels (with different target, pose, etc., values) at each lookup table entry.

1. For each model Object do 2
   2. For each model Azimuth do 3, 4, 5
      3. Obtain the location (R, C) and magnitude (S) of the strongest N scatterers.
      4. Order (R, C, S) triples by descending S.
      5. For each origin O from 1 to N do 6
         6. For each point P from O+1 to N do 7, 8
            7. $dR = R_P - R_O$; $dC = C_P - C_O$.
            8. At look-up table location dR, dC append to list entry with: Object, Azimuth, R_O, C_O,S_O, S_P.

Figure 2.9. Model construction algorithm.

The recognition algorithm is outlined in Figure 2.10. The recognition process uses the relative locations of the N strongest scattering centers in the test image to access the look-up table and generate votes for the appropriate object, azimuth, range, and cross-range translation. (In contrast to many model-based approaches to recognition [21], we are not "searching" all the models.) Further comparison of each test data pair of scatterers with the model look-up table result(s) provides information on the magnitude changes (between the data and the model) for the two scatterers. Limits on allowable values for translations and magnitude changes are used as constraints to reduce the number of false matches. The number of scattering centers used and the various constraint limits are design parameters that are optimized, based on experiments, to produce the best recognition results. (Another approach to optimizing these tuning parameters, based on reinforcement learning is presented in [22].) Given the MSTAR targets are "centered" in the chips, a ± 5 pixel limit on allowable translations is imposed for computational efficiency. The experimentally determined optimum limit on the allowable percent difference in the magnitudes of the data and model scattering centers was $\pm 9\%$, which is consistent with the measured probability mass functions of scatterer magnitude invariance with target configuration variants and articulations (previously shown in Figures 2.8 and 2.7). To accommodate some uncertainty in the scattering center locations, the eight-neighbors of the nominal range and cross-range relative location are also probed in the look-up table, and the translation results are accumulated for a $3*3$ neighborhood in the translation subspace. A city-block weighted voting method reduces the

impact of the more common small relative distances. The recognition process is repeated with different scattering centers as basis points, providing multiple "looks" at the model database to handle spurious scatterers that arise due to articulation, occlusion, or configuration differences. The recognition algorithm actually makes a total of $9N(N-1)/2$ queries of the look-up table to accumulate evidence for the appropriate target type, azimuth angle, and translation. The models (labels with object, azimuth, etc.) associated with a specific look-up table entry are the "real" model and other models that happen by coincidence, to have a scatterer pair with the same (range, cross-range) relative distance. The constraints on magnitude differences filter out many of these false matches. In addition, while these collisions may occur at one relative location, the same random object-azimuth pair doesn't keep showing up at other relative locations with appropriate scatterer magnitudes and mapping to a consistent 3∗3 neighborhood in translation space, while the "correct" object does.

1. Obtain from test image the location (R, C) and magnitude (S) of N strongest scatterers.
2. Order (R, C, S) triples by descending S.
3. For each origin O from 1 to N do 4
  4. For each point P from O+1 to N do 5, 6
    5. $dR = R_P - R_O$; $dC = C_P - C_O$.
    6. For DR from $dR - 1$ to $dR + 1$ do 7
      7. For DC from $dC - 1$ to $dC + 1$ do 8, 9, 10
        8. weighted_vote = |DR| + |DC|.
        9. Look up list of model entries at DR, DC.
        10. For each model entry E in the list do 11
          11. IF $|\text{tr} = R_O - R_E| <$ translation_limit
              and $|\text{tc} = C_O - C_E| <$ translation_limit
              and $|1 - S_{EO}/S_O| <$ magnitude_limit
              and $|1 - S_{EP}/S_P| <$ magnitude_limit
              THEN increment accumulator array [Object, Azimuth, tr, tc]
                by weighted_vote.
12. Query accumulator array for each Object, Azimuth, tr and tc, summing the votes in a 3x3 neighborhood in translation subspace about tr, tc; record the maximum vote_sum and the corresponding Object.
13. IF maximum vote_sum > threshold
    THEN result is Object ELSE result is "unknown."

Figure 2.10. Recognition algorithm

The basic decision rule used in the recognition is to select the object-azimuth pair (and associated "best" translation) with the highest accumulated vote total. To handle identification with "unknown" objects, we introduce a criteria for the quality of the recognition result that the votes for the potential winning object exceed some minimum threshold $v_{\min}$. By varying the

decision rule threshold we obtain a form of receiver operating characteristic (ROC) curve with probability of correct identification, PCI = P\{decide correct object|object is true\}, vs. probability of false alarm, P_f = \{decide any object|unknown is true\}. We call the algorithm a 6D recognition algorithm since, in effect, we use the range and cross-range positions and the magnitudes of pairs of scattering centers. (When using 40 scatterers, this 6D algorithm takes an average of 2.5 seconds to process a test chip on a Sun Ultra2 without any optimizations.)

More formally, a radar image of object c at azimuth pose a consists of N (or more) scatterers, each scatterer k with a magnitude S_k and range and cross-range locations R_k and C_k, which (for consistency) are ordered by decreasing magnitude such that $S_k \geq S_{k+1}$ where $k = 1, \ldots, N$. A *model* M of object c at azimuth a is given by

$$M(c,a) = \{V_1(c,a), V_2(c,a), \ldots, V_{N(N-1)/2}(c,a)\}, \tag{2.1}$$

which is comprised of the set of all pairwise *observations*, V_i,

$$V_i(c,a) = \{f_1, f_2, \ldots, f_6\}_i, \tag{2.2}$$

where $i = 1, 2, \ldots, N(N-1)/2$, $f_1 = R_P - R_O$, $f_2 = C_P - C_O$, $f_3 = R_O$, $f_4 = C_O$, $f_5 = S_O$, $f_6 = S_P$, and with the individual scatterers in each pair labeled O and P so that $S_O \geq S_P$ for consistency (see Figure 2.11).

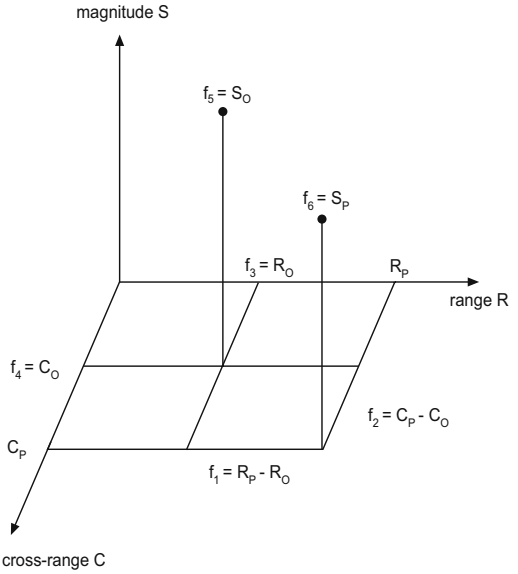

Figure 2.11. Observation for a pair of scatterers O and P.

We define a *match*, H, as

$$H(V_i, V_j) = \begin{cases} w \text{ if } |(f_b)_i - (f_b)_j| \leq \delta_b, \ \forall\, b = 1, \ldots, 6, \\ 0 \ \text{ otherwise} \end{cases} \tag{2.3}$$

where the weight $w = |(f_1)_i| + |(f_2)_i|$ and the match constraints are $\delta_1 = \delta_2 = 0$ pixels, $\delta_3 = \delta_4 = 5$ pixels and $\delta_5 = \delta_6 = L$ percent.

The recognition result, T, for some test image (with a test class, x, and test azimuth, y, to be determined) is a maximal match that is greater than a threshold, D, given by

$$T = \begin{cases} [c, a] \text{ , if } \arg\max_{c,a,t} \left(\sum_{l=1}^{9} \sum_{k=1}^{N(N-1)/2} \sum_{n=1}^{9} H_t^l(V_k^n(x, y), V_m(c, a)) \right) > D, \\ \text{“unknown,” otherwise} \end{cases} \tag{2.4}$$

where $V_m \in M(c, a)$ $\forall m$ such that $|(f_1)_{V_k^n} - (f_1)_{V_m}| = 0$ and $|(f_2)_{V_k^n} - (f_2)_{V_m}| = 0$, and the subscript t applied to a match denotes that the match, H_t, is associated with the relative translation $t(R, C) = (\Delta f_3, \Delta f_4)$ of the stronger scatterers in the two observations. Note that in this formulation the constraint on m avoids exhaustive search of all the models and can be implemented as a look-up table. The nine observations (denoted by the superscript n in V_k^n) are made to account for location uncertainty by taking the 3∗3 neighbors about the nominal values for the relative locations f_1 and f_2 of scatterer pair k in the test image. Similarly, the nine matches (denoted by the superscript l in H_t^l) are computed at the 3∗3 neighbors located ±1 pixel about the resulting nominal value for translation, $t(R, C)$, of the scatterers in the test image from the model.

2.4 Incorporation of Additional Features

A traditional approach to improving recognition performance is to find additional features that distinguish between the objects. The basic SAR recognition system, the 6D system described in Section 2.3, successfully evolved from an earlier simpler 2D version, [12] that used only relative distances and the “exact match” scatterer locations. The 6D version adds: (1) the scatterer magnitudes as additional features; 2) the within-one-pixel quasi-invariance of scatterer locations; and (3) the consistent translation constraint.

In addition to the scattering center locations and magnitude features, a “shape factor” can be used as a measure of the sharpness of the local peak in the radar return associated with a scattering center. We define the shape factor $F = S_k / \sum_{i=1}^{8} S_i$, where S_k is the amplitude of the peak and the S_i's are the amplitudes of the eight neighbors. Figure 2.12 shows the PMFs for percent shape factor change for the strongest 40 scattering centers of T72 #812 vs. #132 (at 15° depression angle). Curves are shown both for cases where the scattering center locations correspond within one pixel tolerance and for all the combinations of scatterers whose locations do not match. For the cases with locations that match within one pixel, the percent shape factor change

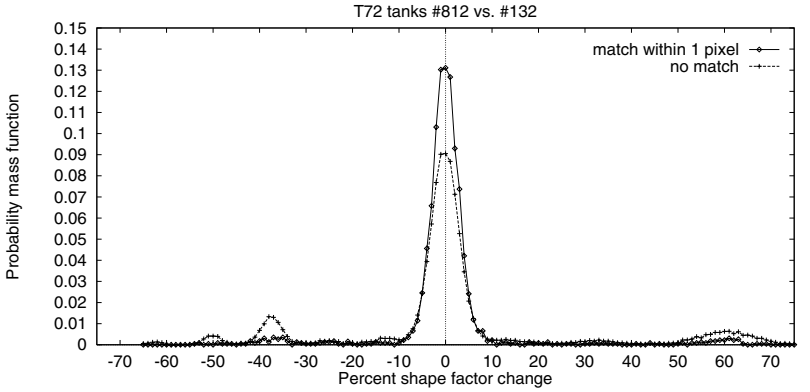

Figure 2.12. Shape factor change with configuration.

mean and standard deviation are 1.3 and 15.7, while for the nonmatching cases they are 5.3 and 31.3, respectively.

The peak shape factors can be used as additional features to create an 8D version of the basic recognition system in a manner similar to the way that the magnitudes of the peaks are handled in the 6D system. Figure 2.13 shows ROC curves for the MSTAR T72 and BMP2 configuration variants with the BTR confuser using the 2D, 6D, and 8D recognition systems. Each of the systems was optimized for the forced recognition configuration variant case: the 2D system at 20 scatterers; the 6D system at 36 scatterers (with ±5 pixel translation and ±9% amplitude change limits); the 8D system at 50 scatterers (with a ±30% shape factor change limit). Both the 6D and 8D system results are a substantial improvement over the earlier 2D system results. While Figure 2.13 shows that the 8D system gave worse results than the 6D system in the region below 0.1 P_f, reoptimizing the operating parameters (e.g., using 45 scatterers) gives the 8D system better results in the region below 0.1 P_f at the cost of a slightly reduced forced recognition rate.

2.5 Exploitation of Model Similarity

2.5.1 Similarity Measurement

Model similarity can be measured in terms of collisions *collisions*, where a collision is an instance when observations of two different objects map into the same location (within some specified region of uncertainty) in feature space, i.e., if $H(V_i, V_j) = 1$ and $c_i \neq c_j$. The recognition system described in the preceding section has a 6-dimensional (6D) feature space based on the range and cross-range positions and magnitudes of pairs of scatterers (see equation (2.2)). As noted before (in equation (2.1)), the model of an object at some azimuth, with N scatterers, is represented by $N(N-1)/2$ observations

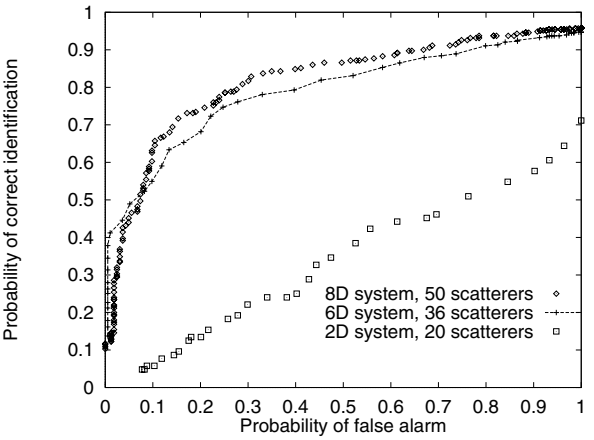

Figure 2.13. ROC curves for configuration variants with 2D, 6D and 8D systems.

using pairs of scatterers with each pair mapped into the 6D feature space. While the 6D feature space could be represented by a simple 6D array in concept, the large range of potential feature values and high dimensionality make other implementations more practical. The nature of the SAR problem, with discrete pixel values for distances and a large dynamic range for scatterer magnitudes, leads to a natural model implementation, shown previously in Figure 2.9, where the relative range and cross-range locations of a scatterer pair are direct indices to a physical 2D array of lists that contain another 4D of information and the label with the object and pose. Thus, the model construction algorithm of Figure 2.9 does not directly provide collisions in all six dimensions of feature space. In order to determine if two objects map to the same location in feature space we need to apply the same constraints as are used in the recognition algorithm (see step 10 of Figure 2.10 and equation (2.3)), because the constraints dictate the size of the region or bucket in feature space that is considered the same location.

The general approach to measure the similarity of one model object with respect to several other objects is to first build the look up table models of the other objects using the normal model construction algorithm of Figure 2.9, and then use a modified version of the recognition algorithm of Figure 2.10 with the subject model object (at all the modeled azimuths) as the test conditions to obtain a histogram of the number scatterer pairs that have various numbers of collisions. Basically the modified algorithm uses the first ten steps of Figure 2.10, with the consideration of each pair of scatterers as a separate occurrence (starting a new count of collisions at step 5) and if the constraints are satisfied (at step 10) then a collision is counted. The total number of observations is equal to $AN(N-1)/2$, where A is the number of azimuths modeled (some of the MSTAR data was sequestered, so not all 360° were available).

Figure 2.14 shows example model collision histograms (at $N = 39$ and $L = 9$) for four MSTAR vehicles (at 15° depression angle): BMP2 armored personnel carrier (APC) serial number (#) c21; BTR70 APC #c71; T72 tank #132 and ZSU23/4 anti-aircraft gun #d08. Note that the ZSU23/4 has significantly fewer collisions with the other vehicles, because the ZSU23/4 SAR scatterers cover a larger area than the other objects, and thus, have fewer collisions.

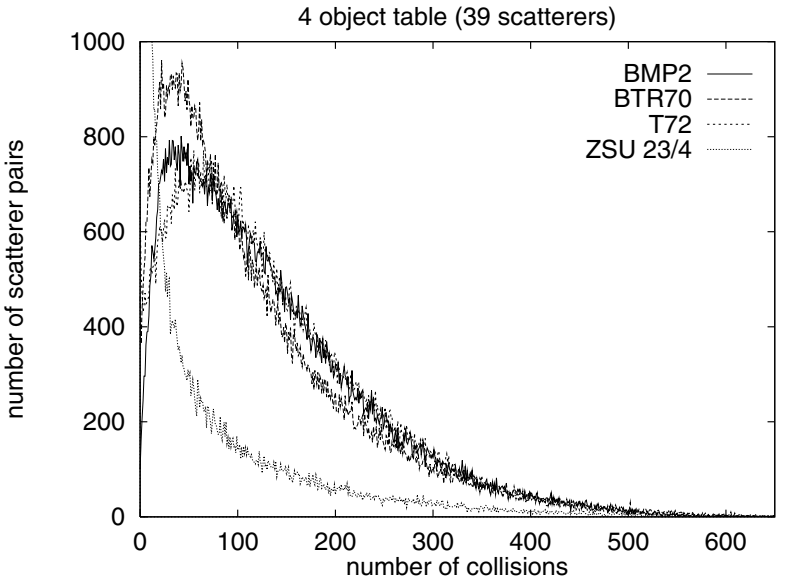

Figure 2.14. Example recognition model look-up table collision histograms.

The similarity of a pair of scatterers of given object (at a given azimuth) to the other objects modeled can be measured by the number of collisions with other objects in the look-up table. This can be expressed as a relative measure by using the collision histogram. For convenience, the population of collisions for a particular object is mapped into equal partitions (each with 10% of the total number of collisions). As an example, for the collision histograms in Figure 2.14 we obtain the results in Table 2.1, which shows the number of collisions for a given percent of the population. For the BMP2, for example, 27 collisions or less is in the 10% of the population that is the least similar to the other three models (whereas 90% of the BMP2 scatterer pairs have 274 or less collisions).

2.5.2 Weighted Voting

The a priori knowledge of the similarities between object models, expressed as the number of collisions for a given percent of the population, can be captured

Table 2.1. Number of collisions for a given percent of the population (example for $N = 39$, $L = 9$).

Object	Number of collisions									
BMP2	27	46	66	87	110	136	167	209	274	676
BTR70	21	37	53	70	91	116	148	192	266	712
T72	27	48	68	89	111	137	168	209	271	667
ZSU 23/4	0	0	0	0	0	1	3	18	78	760
Population percent	10	20	30	40	50	60	70	80	90	100

by assigning weighted votes to model entries in the look-up table, based on collisions with other objects. This is accomplished off-line by again using a version of the recognition algorithm to obtain the number of look-up table collisions for a particular observation with a pair of scatterers from a subject model and azimuth, as before, and then based on the number of collisions determine the population partition (e.g., using Table 2.1) and finally a given weight function is used to assign a weight label to that instance of the particular model observation entry in the look-up table. Thus, in this approach the model similarities, collisions and associated weightings are all precomputed and appropriate weightings are stored in the look-up table during the off-line modeling process. The similarity-weighted models are obtained using the weighted version of an observation (similar to equation (2.2)) given by

$$\hat{V}_i(c, a) = \{w, f_1, f_2, \ldots, f_6\}_i, \tag{2.5}$$

where w is the weight. The similarity weighted version of a match (similar to equation (2.3)), given by

$$\hat{H}(V_i, \hat{V}_j) = \begin{cases} w \text{ if } |(f_b)_i - (f_b)_j| \leq \delta_b, \ \forall\, b = 1, \ldots, 6 \\ 0 \ \text{ otherwise} \end{cases} \tag{2.6}$$

can be substituted in equation (2.4) to obtain weighted recognition results. The various weight functions, used in this research to specify w, are shown in Figure 2.15 which plots the weight value assigned vs. percent of collision population. Function 1 (Figure 2.15(a)) applies equal weight to all the values and is later referred to as unweighted. Functions 2–4 (Figures 2.15(b)–(d)), the convex weight functions, penalize the most similar features (in the right tail of the histogram). Function 5 (Figure 2.15(e)), with equal steps is linear. While functions 6–7 (Figures 2.15(f)–(g)), which reward uniqueness (the left tail of the histogram) are concave. These weight functions illustrate a range of possibilities from function 2, which penalizes only the most similar 10% of the population, to function 7, which rewards only the most dissimilar 10%. These seven weight functions are used and comparative performance results are obtained in experiments described in the next subsection.

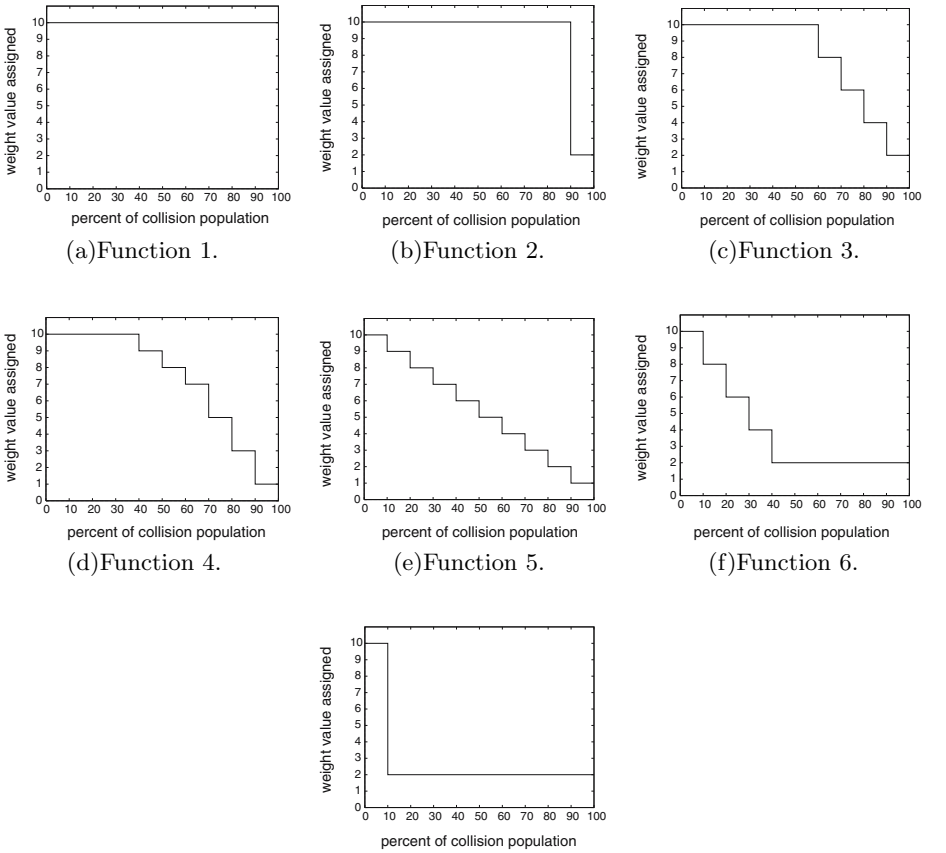

(a)Function 1. (b)Function 2. (c)Function 3.

(d)Function 4. (e)Function 5. (f)Function 6.

(g)Function 7.

Figure 2.15. Table weighting functions.

2.5.3 Configuration Variant Experiments

Our previous results [9] (using a distance-weighted voting technique where the weight was proportional to the sum of the absolute values of the relative range and cross-range distances between the scatterer pair) showed that for the real vehicles used in the MSTAR data, the differences of configurations for an object type are a more significant challenge for recognition than articulation (where the model and the test data are the same physical object under different conditions). Similarly, the previous results [11] on occluded objects (using an unweighted voting technique) demonstrated significantly better recognition results than the configuration variant cases. For these reasons, in this research we follow a similar approach and optimize the recognition system for the difficult configuration variant cases and then utilize the same system parameters for the articulation and occlusion cases. In these (15° depression

angle) configuration variant experiments, the two object model cases use T72 tank #132 and BMP2 APC #C21 as models, while the four object model cases add BTR70 APC #c71 and ZSU23/4 gun #d08. The test data are two other variants of the T72 (#812, #s7) and two variants of the BMP (#9563, #9566). In addition, BRDM2 APC #e71 is used as an unknown confuser vehicle.

The forced recognition results for MSTAR configuration variants are shown in Figure 2.16 for both two object and four object look up table models using various weight functions (defined earlier in Figure 2.15). These results use the optimal parameters (N,L) for each weight function and table size. For the two object cases, function 3 gives the best results, a recognition rate of 95.81%, compared to the unweighted case of 95.17%. For the four object cases, the convex and linear weighting functions all provide better forced recognition performance than the unweighted case. The concave weighting functions result in worse performance than the unweighted case. The best four object result is 94.17% for function 2, compared to the unweighted case of 92.27%. Thus, increasing the number of objects modeled from two to four, reduces the forced recognition rate by 2.9% (95.17 - 92.27) for the unweighted case, while using model similarity information in the optimum weight function reduces that loss to 1% (95.17 - 94.17).

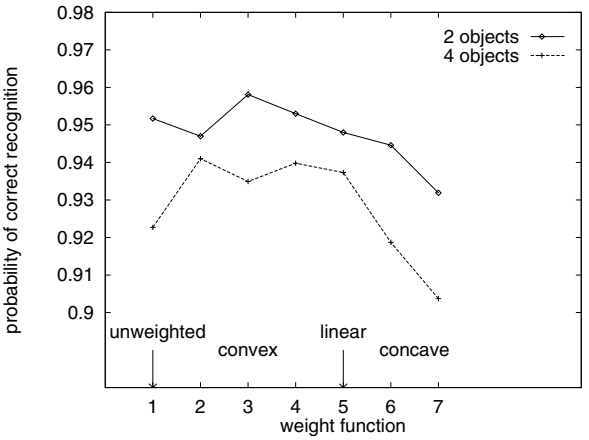

Figure 2.16. Effect of table size and weighting function on forced recognition of MSTAR configuration variants.

Table 2.2 shows example confusion matrices that illustrate the effect of going from a two object recognition system to a four object model recognition system for the MSTAR configuration variant data. In both cases the system parameters (N,L) are optimized for forced recognition (2 objects at (38,11) and 4 at (38,12)), both are unweighted cases (constant weight of 10), and both are for $d = 1700$. (At least 1700 votes, with a weight of 10, is equivalent

to 19 or more scatterers that "matched".) Comparing the two object results on the left of Table 2.2 with the four object results on the right, we observe that basically a large number of confusers and a few targets move from the Unknown column to the additional models. Thus, while the recognition results are similar for 2 and 4 models (PCI = 0.773 and 0.790 respectively) there are increased false alarms (P_f = 0.13 and 0.32 respectively) which would move the knee of the ROC curve to the right.

Table 2.2. Effect of 2 and 4 models on MSTAR configuration variant confusion matrices (unweighted, $d = 1700$).

	Identification results (config. modeled)			Identification results (configuration modeled)				
test targets [serial number]	BMP2 (#C21)	T72 (#132)	Unk.	BMP2 (#C21)	T72 (#132)	BTR70 (#C71)	ZSU23/4 (#d08)	Unk.
BMP2 [#9563,9566]	189	3	25	189	2	8	0	18
T72 [#812,s7]	8	131	58	11	138	1	0	47
BRDM2 (confuser)	28	4	214	27	5	47	0	167

Table 2.3 shows an example MSTAR configuration variant four object confusion matrix for weight function 4. The system parameters (37,9) are optimized for forced recognition with weight function 4 and a d of 1100 is chosen to yield a PCI of 0.776, which is similar to the results shown in Table 2.2. (At least 1100 votes, with an average weight for function 4 of 7.3, is equivalent to 18 or more scatterers matched.) Comparing the earlier four-object unweighted results, shown on the right of Table 2.2, with the weighted results of Table 2.3, we observe that half the misidentifications (11 of 22) are moved to the unknown column. This reduction in misidentifications shows that the model-weighting approach is increasing the distinguishability of the modeled objects. This reduction in misidentifications does not show up directly in the ROC curve results, which treat the off-diagonal target misidentifications the same as the misses where a target is called unknown (i.e., both are cases where the target was not correctly identified). However, the weight function (which effectively reduces the average weighting) allows a similar PCI to be achieved with a lower vote threshold (1100 votes vs. 1700 votes) and results in fewer false alarms. Thus, the lower P_f of 0.276 for the weighted case, vs. 0.321 for the unweighted case, would move the ROC curve to the left.

ROC curves are generated for the four-object configuration variant cases by using the optimum parameters for the forced recognition case and varying the vote threshold. Figure 2.17 shows that the ROC curves for the convex and linear weight functions provide generally better performance than the unweighted case. In addition, Figure 2.18 shows that the concave weight functions give worse performance than the unweighted case (except for the region

Table 2.3. Example MSTAR configuration variant confusion matrix for weight function 4 ($d = 1100$).

test targets [serial number]		Identification results (configuration modeled) BMP2 (#C21)	T72 (#132)	BTR70 (#C71)	ZSU23/4 (#d08)	Unknown
BMP2	[#9563,9566]	179	6	1	0	32
T72	[#812,s7]	4	143	0	0	50
BRDM2 (confuser)		30	6	32	0	178

where PCI < 0.5, $P_f < 0.05$). The convex weight functions penalize the most common features and so are not much affected by noise (due to configuration differences or other confuser vehicles). On the other hand, the concave weight functions reward (very strongly reward in function 7) the relatively unique features, which makes them susceptible to conditions where noise is strongly rewarded.

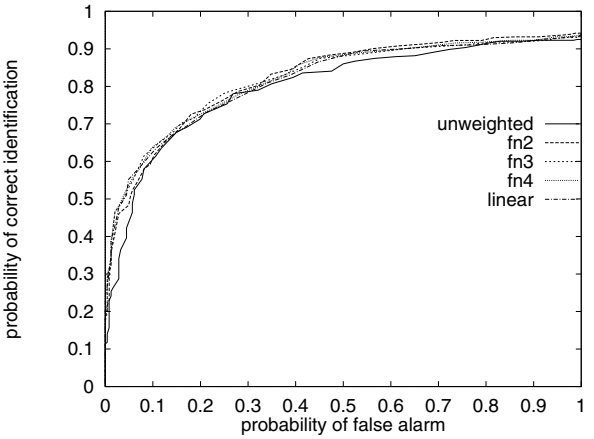

Figure 2.17. MSTAR configuration variant ROCs for beneficial weight functions (four objects).

2.5.4 Articulation Experiments

In the articulation experiments the models are nonarticulated versions of T72 #a64 and ZSU23/4 #d08 and the test data are the articulated versions of these same serial number objects and BRDM2 #e71 as a confuser vehicle (all at 30° depression angle).

Figure 2.19 shows the ROC curves, with excellent articulated object recognition results for both the weight function 2 and the unweighted cases. Since

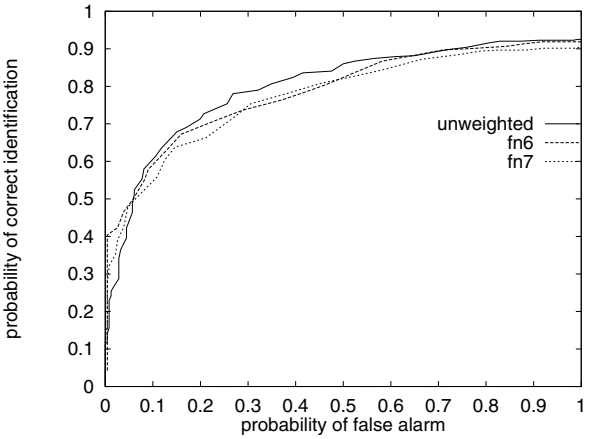

Figure 2.18. MSTAR configuration variant ROCs for concave weight functions (four objects).

weight function 2, with $N = 39$ and $L = 9$, gives the optimum ROC results for the two object (T72, BMP2) configuration experiments and the optimum unweighted parameters are $N = 38$ and $L = 11$, these same parameters are used for the articulation experiments.

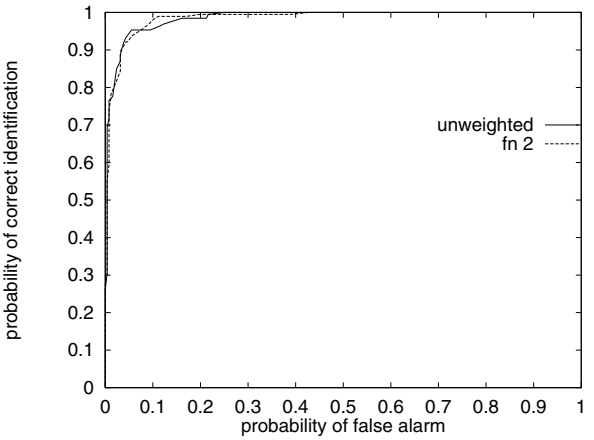

Figure 2.19. Articulation recognition results.

2.5.5 Occlusion Experiments

The occlusion experiments use the same four models as the configuration variant experiments: T72 tank #132, BMP2 APC #C21, BTR70 APC #c71 and ZSU23/4 gun #d08 (all at 15° depression angle). The occluded test data is

generated using the technique described previously in Subsection 2.2.3. In our previous work on occluded objects [11], the confuser vehicle was occluded. However, while the target may be occluded, the confuser vehicle may not necessarily be occluded in practical situations. Hence, in this case the BRDM2 APC (#e71) is an *unoccluded confuser* vehicle, which is a more difficult problem.

Figure 2.20 shows the effect of occlusion on ROC curves for weight function 2, with $N = 40$ and $L = 9$ (while $N = 40$ is not optimum, it yields occlusion in 5% increments). Here with the unoccluded confuser, excellent recognition results are achieved for less than 45 percent occlusion, compared with the prior 70 percent occlusion with an occluded confuser [11].

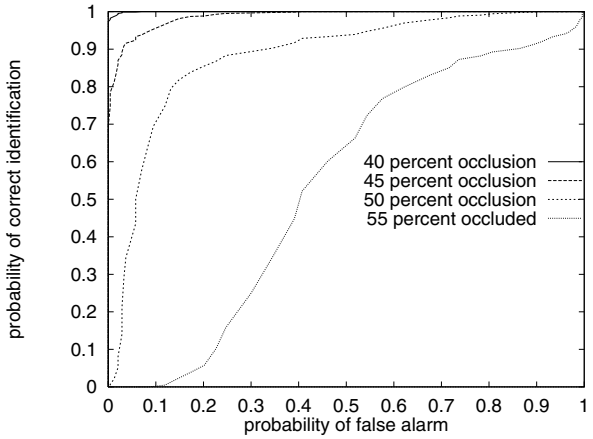

Figure 2.20. Effect of occlusion on receiver operating characteristics.

2.6 Multiple Recognizers at Different Look Angles

2.6.1 Independence of Multiple Look Angle SAR Recognizers

The azimuthal variance of SAR scatterer locations, previously demonstrated in Figure 2.4, strongly indicates that observations at different azimuth angles are independent. Given the probability of one SAR recognizer failing, $F1$, where $F1 = 1 - PCI$; then if two recognizers are independent, the probability that both recognizers are wrong, $F2$, is simply $F2 = F1^2$. In order to obtain the most failures, we pick the object configuration variant case, which is the most difficult case for our SAR recognition approach, compared to the depression angle change and object articulation cases.

In the configuration variant experiments a single configuration of the T72 (#132) and BMP2 (#C21) vehicles are used as the models and the test data

are two other variants of each vehicle type (T72 #812, #s7 and BMP2 #9563, #9566), all at 15° depression angle. These results are obtained using the optimum parameters of 38 scattering centers and a percent magnitude change of less than ±11%. These parameter settings are slightly different from the corresponding (36 and 9%) values used previously in Section 2.4, because here we use unweighted voting, as opposed to the previous distance-weighted voting method. Figure 2.21 takes the experimental forced recognition results for the configuration variant cases with all available combinations of two different azimuths and plots the probability that two recognizers are both wrong as a function of the difference in azimuth angle of the object from the two recognizers. (While Figure 2.21 emphasizes the small angles by only showing up to ±60 degrees, the results out to ±180 degrees are similar.) The single recognizer result, 19 failures in 414 trials, is an F1 failure rate of 0.0459, which is plotted for reference as point "a" in Figure 2.21. For an F1 of 0.0459 the predicted value of F2 is 0.0021, which is very close to the overall experimental average F2 of 0.0025 . The other interesting observation from Figure 2.21 is that the results are independent of the angle difference, even for very small values like 1 degree. This demonstration that multiple-look-angle SAR recognition results are independent, even for small angles down to 1 degree, provides the scientific basis for both measuring and improving the quality of recognition results.

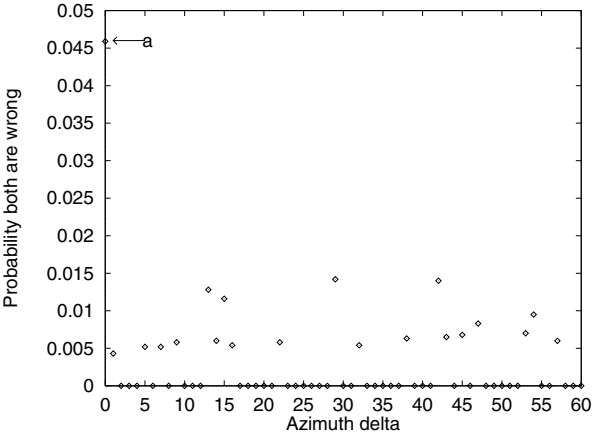

Figure 2.21. Probability that two recognizers are both wrong.

2.6.2 Multiple-Look-Angle Configuration Variant Results

In contrast to the forced recognition case described in the previous subsection, in these configuration variant experiments the BTR70 armored personnel carrier (#c71) is used as an unmodeled confuser vehicle to test the recognition

system and the vote threshold parameter is used to generate "unknown" results. The other test conditions and parameters are the same as the forced recognition case (most significantly, the models are one configuration of the T72 and BMP2 vehicles and the test vehicles are two different configurations).

Figure 2.22 shows the effect of multiple look angle recognizers on the probability of false alarm using the BTR70 as a confuser. (The BTR70 is a more difficult case than other confusers such as the BRDM2 armored personnel carrier or the ZSU 23/4 anti-aircraft gun [9].) In the cases with two recognizers, the decision rule is that if either gives results above the vote threshold, the result is declared a target (which, for these BTR70 confusers, would be a false alarm). Thus, with this "target bias" decision rule the multiple recognizer cases have higher false alarms than a single recognizer. It is important to note that the penalty in increased false alarms is small for the left tail of the curve. Figure 2.22 also shows that the false alarm rates are similar for all the two-look angle recognizer cases and that agreement on the "target" is basically irrelevant for a false alarm.

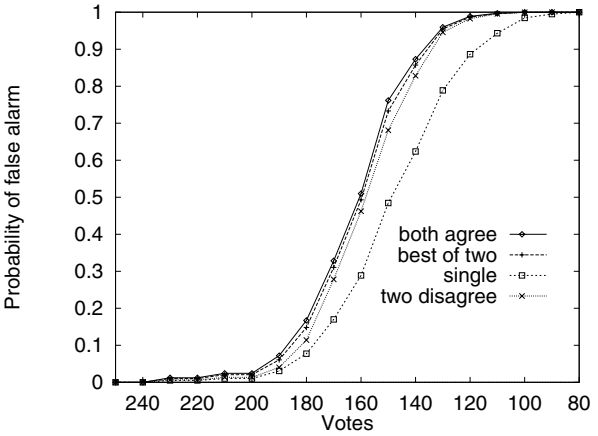

Figure 2.22. Effect of multi-look on probability of false alarm.

Figure 2.23 shows the effect of multiple-look-angle recognizers on the probability of correct recognition for the configuration variant case where the test data are different configurations of the T72 and BMP2. The top curve shows the results for the 91.7 percent of the time when two recognizers at different look angles agree on the result. The bottom curve is for the remaining 8.3 percent of the time when the two recognizers disagree and the answer that gets the most votes is chosen. The second curve, labeled "best of two," uses a decision level fusion rule that simply picks the target based on which of the two recognizers got the most votes. (This case is also the weighted average of the agree and disagree cases). In Figure 2.23 the probability of correct recognition decreases as the vote threshold increases (to the left in Figure 2.23), because

the higher threshold causes more targets to be classified as "unknown." The recognition results for using the best of two recognizers at different look angles are substantially better than the results for a single recognizer. This is basically the result of fewer "misses," where a target object is classified as an "unknown"; because there are two opportunities to get above the vote threshold and declare a "target."

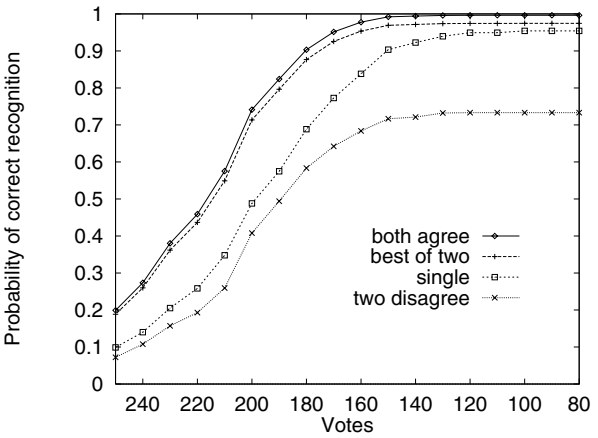

Figure 2.23. Effect of multi-look on probability of correct recognition.

Figure 2.24 combines the results of Figures 2.22 and 2.23 and shows the effect of using multiple-look-angle recognizers on the ROC curve for the configuration variant cases. These recognition results, using the best-of-two recognizers at different look angles, are substantially better than the results for a single recognizer. For example, at a 0.10 P_f the PCI for the best of two look angles is 0.8324, compared to 0.7091 for a single recognizer. The performance improvement is because the cost in increased false alarms (in Figure 2.22) is low compared to the benefits in increased recognition (in Figures 2.23), due to fewer targets being classified as "unknown."

2.6.3 Multiple-Look-Angle Articulation Results

In the articulated object experiments the models are nonarticulated versions of T72 tank #a64 and ZSU 23/4 anti-aircraft gun #d08 (with the gun turret straight forward) and the test data are articulated versions of these same serial number objects (with the turret rotated) and BRDM2 armored personnel carrier #e71 as a confuser vehicle (all at 30° depression angle). The results of applying the same techniques (and all the same recognition system parameters) in these articulated object experiments are shown as ROC curves in Figure 2.25. Again the results for using two recognizers at different look angles and picking the answer with the largest number of votes are better than the single recognizer results.

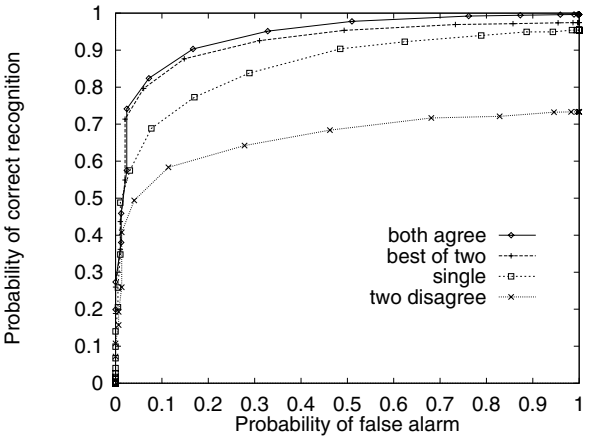

Figure 2.24. Effect of multilook on configuration variant ROC curve.

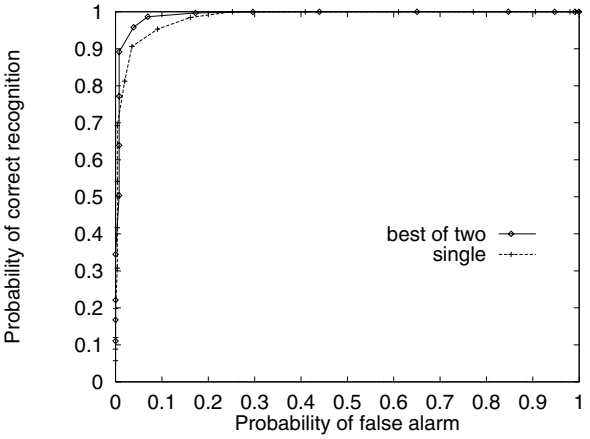

Figure 2.25. Effect of multilook on articulated object ROC curve.

2.6.4 Multiple-Look-Angle Occlusion Results

The occlusion experiments use four models: T72 tank #132, BMP2 APC #C21, BTR70 APC #c71 and ZSU23/4 gun #d08 and the unmodeled confuser vehicle is BRDM2 APC (#e71) (all at 15° depression angle). The occluded test data is generated using the technique described previously in Subsection 2.2.3, while the BRDM2 APC (#e71) is the more difficult *unoccluded confuser* vehicle.

Figure 2.26 shows the effect of multiple-look-angle recognizers on the probability of correct recognition for the case of 50% occluded targets and an unoccluded confuser. The same techniques (and all the same recognition system parameters) used in the prior configuration variant and articulation experiments are applied to these occluded object experiments. Here again, using two recognizers at different look angles and a decision-level fusion rule of picking

the answer with the largest number of votes gives better results than a single recognizer.

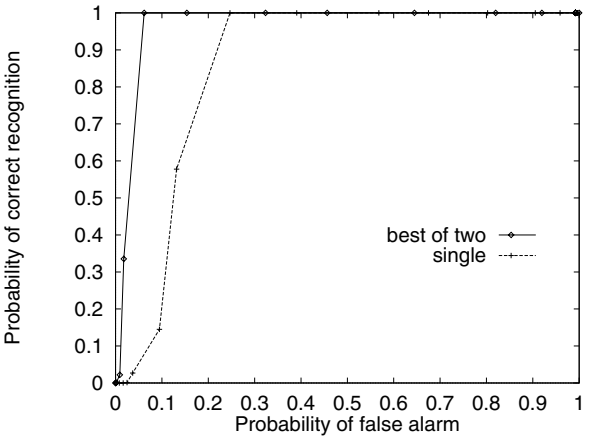

Figure 2.26. Effect of multi-look on 50% occluded object ROC curve.

2.7 Conclusions

The locations and magnitudes of a significant number of SAR scatterers are quasi-invariant with target configuration variations and articulations. A model-based recognition system, using inexact match of local features can successfully handle difficult conditions with object configuration variants, articulation, and occlusion. A comparison of experimental recognition results for MSTAR configuration variants is shown in Table 2.4 for different methods of improving performance of SAR recognition systems involving incorporation of additional features; exploitation of knowledge of model similarity; and integration of multiple recognizers at different look angles. Recognition rates are shown for forced recognition cases and for cases with a 0.10 confuser false alarm rate.

The use of additional scatterer magnitude features, the consistent translation constraint, and the ability to handle inexact matches of these local features are fundamental to the success of the basic 6D recognition system, compared to the earlier 2D system [12] which only used relative scatterer locations and required an exact location match. Additional quasi-invariant features, such as peak shape factor in the 8D system, can provide some increase in recognition performance.

The similarities between object models can be effectively quantified using histograms of collisions in feature space. This a priori knowledge of object similarity can be successfully used to improve the performance of SAR target

Table 2.4. Comparison of results for MSTAR T72 and BMP2 configuration variants (6D systems, except as noted by *).

	recognition rate	
	forced	at 0.10 P_f
Additional features [Figure 2.13]:		
* 2D system	0.712	0.058
6D system	0.947	0.554
* 8D system	0.957	0.636
Use model similarity:		
function 2 [Figure 2.17], 4 models	0.942	0.609
2 models	0.949	0.744
Multiple look angles:		
best of two [Figure 2.24]	0.975	0.832

recognition. The approach can increase the distinguishability of the modeled objects, reduce misidentifications, and result in decreased false alarms. This is especially beneficial in cases where the number of modeled objects is large. One set of results shown in Table 2.4 for "model similarity" is for a more difficult case with four models, while all the other cases in the table are for two models. In the most difficult configuration variant cases, the convex and linear weight functions, which penalize the most common features, give better performance than the concave weight functions, which strongly reward relatively unique features.

The fundamental azimuthal variance of SAR scatterer locations can be successfully used as the basis for a principled and effective multiple-look-angle SAR recognition approach. The experiments demonstrate that SAR recognition results at different azimuths are independent, even for small azimuths, such as one degree. In addition, using decision level fusion of two observations at different look angles can substantially increase SAR recognition performance for target configuration variants.

These techniques have also been successfully applied to recognition of articulated objects and occluded objects. In experiments using MSTAR SAR data with a BRDM2 APC confuser and articulated versions of a T72 tank and ZSU 23/4 anti-aircraft gun, the basic 6D recognition system with non-articulated T72 and ZSU 23/4 models achieved a $95.6-95.7\%$ recognition rate (depending on system parameters) with a 0.10 P_f. Comparable rates using the model similarity and multiple-look-angle approaches increased to 98.0% and 99.0% respectively (see Figures 2.19 and 2.25). Similarly, for experiments with 50 percent occluded objects (with an unoccluded confuser), using the model similarity approach achieved a 70.1% recognition rate at $0.10P_f$ and multiple look angles achieved 100%, while the basic 6D system only achieved a 20.7% recognition rate (see Figures 2.20 and 2.26).

Higher-resolution SAR data, instead of the one-foot resolution now commonly available, would greatly increase the discriminating power of the current scatterer location and magnitude features. Additional features such as valleys or ridges could also be used, especially with higher-resolution data. The approach of exploiting knowledge of model similarity will become more critical in scaling the recognition problem from 2 to 4 objects to a more realistic 20 to 40 objects. The multiple-look-angle approach could be readily extended to use more than two look angles and more formal methods, like Dempster–Shafer and Bayesian techniques could be used for decision-level fusion. In addition, while the research described in this chapter independently addresses three basic approaches to improve recognition performance: (1) incorporation of additional features; (2) exploitation of a priori knowledge of model similarity; and (3) integration of multiple recognizers at different look angles, these techniques could be combined in practice to address difficult operating conditions involving large numbers of different objects with the combined effects of non-standard configurations, articulation and occlusion.

Acknowledgements

This work is supported by AFOSR grant F49620-02-1-0315; the contents and information do not necessarily reflect the position or policy of the U.S. Government.

References

[1] Ross, T., Worrell, S., Velten, V., Mossing, J., Bryant, M.: Standard SAR ATR evaluation experiments using the MSTAR public release data set. In: SPIE Proceedings: Algorithms for Synthetic Aperture Radar Imagery V. Volume 3370. (1998) 566–573

[2] Carlson, D., Kumar, B., Mitchell, R., Hoffelder, M.: Optimal trade-off distance classifier correlation filters (OTDCCFs) for synthetic aperture radar automatic target recognition. In: SPIE Proceedings: Algorithms for Synthetic Aperture Radar Imagery IV. Volume 3070. (1997) 110–120

[3] Casasent, D., Shenoy, R.: Synthetic aperture radar detection and clutter rejection MINACE filters. Pattern Recognition **30** (1997) 151–162

[4] Meth, R., Chellappa, R.: Automatic classification of targets in synthetic aperture radar imagery using topographic features. In: SPIE Proceedings: Algorithms for SAR Imagery III. Volume 2757. (1996) 186–193

[5] Ryan, T., Egaas, B.: SAR target indexing with hierarchical distance transforms. In: SPIE Proceedings: Algorithms for Synthetic Aperture Radar Imagery III. Volume 2757. (1996) 243–252

[6] Verly, J., Delanoy, R., Lazott, C.: Principles and evaluation of an automatic target recognition system for synthetic aperture radar imagery

based on the use of functional templates. In: SPIE Proceedings: Automatic Target Recognition III. Volume 1960., Orlando, FL (1993) 57–71
[7] Casasent, D., Shenoy, R.: Feature space trajectory for distorted-object classification and pose estimation in SAR. Optical Engineering **36** (1997) 2719–2728
[8] Yi, J.H., Bhanu, B., Li, M.: Target indexing in SAR images using scattering centers and the Hausdorff distance. Pattern Recognition Letters **17** (1996) 1191–1198
[9] Bhanu, B., Jones, G.: Recognizing target variations and articulations in synthetic aperture radar images. Optical Engineering **39** (2000) 712–723
[10] Jones, G., Bhanu, B.: Recognizing articulated targets in SAR images. Pattern Recognition **34** (2001) 469–485
[11] Jones, G., Bhanu, B.: Recognizing occluded objects in SAR images. IEEE Transactions on Aerospace and Electronic Systems **37** (2001) 316–328
[12] III, G.J., Bhanu, B.: Recognition of articulated and occluded objects. IEEE Transactions on Pattern Analysis and Machine Intelligence **21** (1999) 603–613
[13] Boshra, M., Bhanu, B.: Predicting an upper bound on performance of target recognition in SAR images. IEEE Transactions on Aerospace and Electronic Systems **37** (2001) 876–888
[14] : Khoros Pro v2.2 User's Guide. Addison-Wesley-Longman (1998)
[15] Dudgeon, D., Lacoss, R., Lazott, C., Verly, J.: Use of persistent scatterers for model-based recognition. In: SPIE Proceedings: Algorithms for Synthetic Aperture Radar Imagery. Volume 2230., Orlando, FL (1994) 356–368
[16] Novak, L., Halversen, S., Owirka, G., Hiett, M.: Effects of polarization and resolution on SAR ATR. IEEE Transactions on Aerospace and Electronic Systems **33** (1997) 102–115
[17] Ikeuchi, K., Shakungaa, T., Wheelera, M., Yamazaki, T.: Invariant histograms and deformable template matching for SAR target recognition. In: Proc. IEEE Conf. on Comp. Vision and Pattern Rec. (1996) 100–105
[18] Mossing, J., Ross, T.: An evaluation of SAR ATR algorithm performance sensitivity to MSTAR extended operating conditions. In: SPIE Proceedings: Algorithms for SAR Imagery V. Volume 3370. (1998) 554–565
[19] Wissinger, J., Ristroph, R., Diemunsch, J., Severson, W., Freudenthal, E.: MSTAR's extensible search engine and inferencing toolkit. In: SPIE Proceedings: Algorithms for SAR Imagery VI. Volume 3721. (1999) 554–570
[20] Lamden, Y., Wolfson, H.: Geometric hashing: A general and efficient model-based recognition scheme. In: Proc. International Conference on Computer Vision. (1988) 238–249
[21] Grimson, W.E.L.: Object Recognition by Computer: The Role of Geometric Constraints. The MIT Press, Cambridge, MA (1990)
[22] Bhanu, B., Lin, Y., Jones, G., Peng, J.: Adaptive target recognition. Machine Vision and Applications **11** (2000) 289–299